Doorpler : A Radar-based System for Real-Time, Low Power Zone Occupancy Sensing

Avinash Kalyanaraman, Elahe Soltanaghaei, Kamin Whitehouse
University of Virginia
Email: {ak3ka, es3ce, whitehouse}@virginia.edu

***Abstract*—Many homes today are logically or physically "zoned" based on properties such as HVACs, activities, or physical layouts. Accurately sensing the occupancy of these zones can yield energy savings, aid in automatic heating and lighting control, energy disaggregation, etc. Existing systems that attempt to sense occupancy are power consuming, non real-time, pet unfriendly and/or sensitive to ambient heat, light and air flow. In this paper, we address these by building *Doorpler*, a time, space and power-aware radar-based system that detects occupancy at zone transition points by sensing crossings and their direction. It detects a crossing via the *Doppler Principle*, and infers the direction of crossing by measuring the angle-of-arrival of the human reflection. We evaluate *Doorpler* by conducting a scripted study and two in-situ studies for 200 hours, collecting over 1600 doorway crossings. We obtain a precision, recall and direction accuracy of over 99% in the scripted studies, and over 95% in the in-situ studies. Our results estimate that *Doorpler* can fall in the energy-harvestable range of indoor environments with an average power consumption of 6.1mW. With an execution time of 13.8ms, *Doorpler* has the potential to enable several real-time smart home applications like smart-lighting and HVAC control.**

***Index Terms*—Smart Homes, Radar, Wireless Systems, Occupancy Sensing**

I. Introduction

Many homes today are logically or physically "zoned" — based on HVACs [1], tasks performed (rooms), physical layout (floors), etc. A sensing technology that can accurately sense this zone occupancy can obtain energy savings (in the order of 20-30% [2]), perform automatic lighting control (i.e. lights automatically come on when one enters a room, and goes off during an exit in real-time — just like a human would do), aid in energy disaggregation in 35 million single-person households in the US [3], perform elderly monitoring in the 13 million elderly single-person households [4], and help carry out "eyes-off" security (e.g. when a person exits a home through the back door, an unlocked front door locks itself).

The most common off-the-shelf solution for zone occupancy that exists in homes is a motion sensor. However, a single motion sensor has no notion of direction (i.e. it cannot distinguish between a zone crossing and a nearby hover). Furthermore, these motion sensors infer zone exit from lack of motion. Consequently, occupied periods can be mis-classified as unoccupied ("the waving hand at motion sensor problem"), and zone exit events become non real-time. On the other hand, many doorway tracking systems exist in literature [5]–[9] that can sense zone occupancy at zone transition spots (e.g. doorway) by detecting a crossing and the direction of movement. However, these systems are high-power [6]–[9], cannot distinguish between a near-door event (e.g. hover) and a real crossing [5], [7], [8], are pets unfriendly [5], [8], [9], or depend on the ambient lighting, air flow or temperature [10], [11]. Consequently, in this paper we ask the question, how can we build a system that can perform crossing detection and direction estimation at *low-power* (in a harvestable range as most zone transition spots such as doorways do not have a nearby power outlet), in *real-time* and with a small form-factor (since space is at a premium in a doorway), while addressing the above limitations.

To answer this question, we build *Doorpler*, a radar-based sensing system that performs crossing detection and direction estimation using the simplest radio frequency (RF) signal, namely a tone (a continuous wave at a constant frequency), while adhering to the time, space, and power constraints of the application. *Doorpler* is mounted atop a zone transition spot such as a doorway, and detects a crossing by leveraging the *Doppler Effect* — a person walking towards the radar causes an increase in the frequency of the transmitted signal. It estimates the direction of crossing by computing the angle-of-arrival (AoA) of the signal reflected by the human. It leverages the intuition that a person walking through the doorway creates a few "good" reflections where they reflect directly towards the radar [12], and ensures that these reflections are not inundated by the "bad" multi-path reflections coming off the environment. However, unlike many conventional radar direction finding systems which consume time, space, and power [13]–[17], *Doorpler* is *real-time, space-efficient*, and *power-aware* (i.e. within harvestable range). As there is a coarser requirement on the angular accuracy (i.e. we need to differentiate whether the angle of arrival of the human reflection is positive or negative depending on the side of the doorway), *Doorpler* employs an FFT-based technique that trades angular accuracy for computational complexity and relies on the phase difference between pairs of receiver elements. *Doorpler* operates these receiver elements in the 5.8GHz ISM band which allows for a compact array size of 7.8cm. Finally, since the interesting crossing events are sparse, *Doorpler* saves power via a dual-band wake-up radio technique [18], [19]. Accordingly, a lower frequency 2.4GHz radar (and hence lower power) is used for crossing detection, while a triggered higher frequency 5.8GHz (and hence higher power) array performs direction estimation.

To evaluate *Doorpler*, we study its accuracy, power con-

978-1-7281-0678-6/19/$31.00 ©2019 IEEE
DOI 10.1109/RTAS.2019.00012

sumption and real-timeness. We first conducted a scripted study with 8 participants of varying height and weight who were asked to walk through an instrumented doorway in different ways, every day for 6 consecutive days, producing over 1400 doorway crossing events. Our results show that *Doorpler* can achieve a precision, recall and direction accuracy of over 99% accuracy. Next, we performed two in-situ studies for 200 hours, on an instrumented doorway in a lab and a 2-person home, generating nearly 250 crossings. Despite the uncontrolled environment, *Doorpler* achieves an average precision, recall and direction accuracy of 98.7%, 95.4% and 100%, respectively. Next, we estimate that a realization of *Doorpler* when instrumented atop a doorway would consume 6.1mW of power, falling in the harvestable solar range for indoor environments [20]. To evaluate the real-timeness of the system, we implemented the digital baseband processing on an ultra-low power microcontroller. Our results show an execution time of 13.8ms, thus having the potential to enable several real-time smart home applications like smart-lighting, HVAC control.

II. Related Work

At a high-level, *Doorpler* performs real-time crossing detection and direction estimation at zone transition spots, such as doorways (we use the terms zone transition spots and doorways interchangeably). It operates at low-power using just a 100μW tone. *Doorpler* is inspired by existing works in radar-based direction finding systems, doorway tracking systems and indoor RF-based localization systems.

Radars: Radars have long been used to detect targets and their direction by analyzing the reflections of a transmitted signal [21]. However, many of these solutions [22] cannot be directly applied to our use-case, as these systems tend to be space-heavy [13]–[15] (i.e. we want *Doorpler* to have a form-factor that fits onto a doorjamb whose width can be as small as 10cm [23]) or time-heavy [16], [17] (i.e. we want *Doorpler* to be real-time). Examples of space-heavy techniques include Time Difference of Arrival [13], Amplitude-based AoA [14] which require a large antenna separation such that RF path loss difference can be used to determine the direction - a spatial luxury unavailable atop a doorway. On the other hand, time-heavy techniques include those that have a large scan-time [24] or employ subspace techniques [16], [17] that are computationally heavy to run in real-time on an ultra low power microcontroller.

Like other continuous-wave (CW) radar systems, *Doorpler* also works by analyzing the reflections of a transmitted tone signal. However, it adheres to the space, time and power-constraints of the use case. It only requires a coarser angular accuracy (i.e. whether the angle of the reflection from the human is positive or negative depending on the doorway side) in estimating the direction of transition. Consequently, it employs an FFT-based technique that isolates the reflection from the crossing human and trades-off angular accuaracy for computational complexity. The coarse nature of the angular accuracy also eliminates the need for large phased arrays, a common space-heavy direction finding solution [15]. The coarseness also permits *Doorpler* to transmit at very low-power and work with low sampling rates.

Secondly, radars employ different techniques to mitigate direct path interference such as delayed sampling (pulse radars), shadowing or beam-steering [25]. In contrast, *Doorpler* employs a technique by orienting the nulls of the omni-directional transmit and receive antennas towards each other (i.e. antennas point at each other so that the antenna gains mismatch). Consequently, most of the energy is radiated downwards into the doorway, and the direct path is weakened.

Finally, *Doorpler* identifies the moment a person crosses the doorway via a technique inspired by Doppler and pseudo-Doppler direction finders [26]. In such systems, an RF transmitter is localized by a rotating receiver – there will be positive Doppler when the receiver is rotating towards the active RF source, and negative while moving away, with the zero-crossing informing the direction of the RF source. *Doorpler* uses a similar technique but instead of a rotating radio, it leverages the moving human. A person crossing the doorway causes positive and negative Doppler during approach and exit respectively. The zero-crossing thus tells *Doorpler* when the person was underneath the sensor, creating a temporal reference for AoA comparison.

Doorway Tracking Systems: Several doorway tracking systems have been built that can perform crossing detection and direction estimation [5]–[10]. However, these systems either consume high power [6]–[10] (i.e. outside a harvestable limit), are not highly accurate in direction estimation [5], [8], are pet unfriendly (ultrasonic sensors) [5], [9], cannot distinguish between movements near the doorway and doorway crossing events [5], [7] or make assumptions about the heat profile of a human [10], [11]. The current state-of-the-shelf system that is commonly deployed in rooms of homes and offices for our use-case are motion sensors. However, a single motion sensor cannot provide a direction estimate, and movements near the sensor can trigger false positives. Furthermore, these motion sensors are also not real-time, particularly during exit-events (i.e. lack of motion for a period of time is perceived as an exit). Since lack of motion is perceived as exit, occupied periods get mis-classified as unoccupied ("the hand-waving at motion sensor problem"). Finally, motion sensors can also get triggered by external factors such as sunlight, car lights (if used in exterior doorways) or HVAC air flows [27] (a limitation even if they are placed on either side of the doorway). *Doorpler* mitigates the above limitations of both state-of-the-art and state-of-the-shelf systems by using the phase and amplitude of low-power RF signals that cause no harmful effects, distinguishes near-door events from crossing events, and is independent of the lighting, air flow or the heat profile of the person.

RF-based Indoor Localization: Several device-based systems exist that can localize a person indoors with high accuracy using RF signals [28]–[33]. However these systems require a person to carry a device — an issue in homes due to the documented *forget to wear, forget to charge* problem [34].

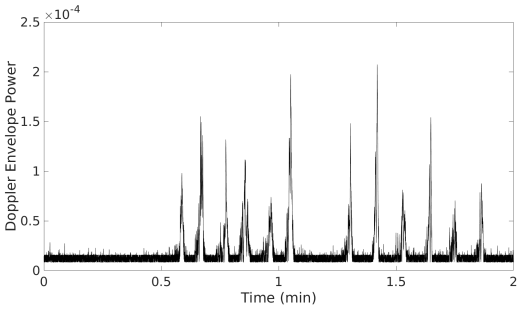

Fig. 1: The envelope of the Doppler signal reflected back to *Doorpler* during a doorway crossing (a peak in the figure) is much larger than that in the absence of a crossing. There are 12 crossings in this figure.

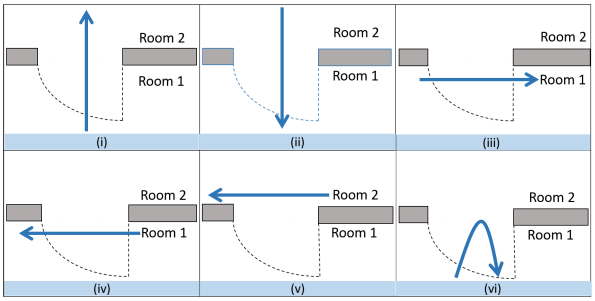

Fig. 2: A positive Doppler shift followed by a negative Doppler shift can occur not only when a person walks through the doorway (cases (i) and (ii), but also due to other movements near the doorway such as hovers and U-turns (cases (iii) - (vi)).

Furthermore, these systems typically analyze the (strongest) direct path, while *Doorpler* is concerned about the weak reflected path coming from the human. There exist systems that use WiFi or Frequency Modulated Continuous Wave (FMCW) radar signals [35]–[38] to localize people in a device-free manner. However the power consumption of these systems is typically higher than CW systems [39], [40] because (i) a CW system is a subset of these systems, (ii) of the lower bandwidth of usage, (iii) of WiFi Orthogonal frequency-division multiplexing's (OFDM) high peak-to-average-ratio [41], (iv) of lack of any protocol overheads (WiFi). Furthermore, as FMCW systems sweep a much larger bandwidth, they are also more prone to interfering RF sources. Finally, we add that systems that use sonar for person or finger localization [42], [43] are also subject to the pet unfriendly limitation like the ultrasonic doorway tracking systems.

III. Approach

Doorpler is a radar-based system mounted atop the doorway. It performs crossing detection and direction estimation using only an RF tone. It detects a crossing by leveraging the Doppler effect – i.e. the receiver observes a shift in the transmitted frequency due to human motion. It estimates the direction of human transition by computing the angle-of-arrival (AoA) of the reflection coming from the human onto an antenna array. To realize this, *Doorpler* takes a layered approach owing to a *space-power* tradeoff. Accordingly, a lower frequency of operation results in a lower power consumption [44]. However, a lower operating frequency also results in a large antenna array that can out-span the door (as the array size depends on the wavelength [15]). In other words, *Doorpler* wants to transmit at a low frequency for power sake but also at a high frequency for spatial benefits. To handle this trade-off, *Doorpler* uses a technique called *dual-band wake up radio* [18], [19] by operating at two different ISM bands (2.4GHz and 5.8GHz). The lower power 2.4GHz radio performs crossing detection and triggers the higher power 5.8GHz array for direction estimation, only when a crossing is detected. We next explain the design details of *Doorpler*.

A. Crossing Detection

In order to detect a crossing event, *Doorpler* relies on the *Doppler Effect*. Accordingly, when a target moves towards the receiver during a radio transmission, the target acts as a virtual transmitter by reflecting the transmitted signal with a frequency larger than the transmitted frequency. This phenomenon is referred to as the *Positive Doppler Effect*. We next describe how this *Positive Doppler* is leveraged by *Doorpler*.

Doorpler uses a 2.4GHz RF transmitter which transmits a carrier signal that is given by [45]

$$x(t) = A\ cos(2\pi f_c t) \tag{1}$$

where A is the transmit signal magnitude and f_c represents the carrier frequency of 2.4GHz. This transmitted signal propagates through air and is received by an antenna placed at the other end of the doorway. This received signal is given by [46]

$$y(t) = \eta A\ cos(2\pi f_c(t-\tau)) \tag{2}$$

where η is the attenuation factor, and τ represents the propagation time. However, the transmitted signal does not travel along just one path from the transmitter to the receiver. The transmitted signal gets reflected by the objects in the environment resulting in multiple copies of the same signal arriving at the receiver. This is referred to as *multipath propagation* and the super-imposed received signal at the receiver due to the N propagation paths is given by

$$y(t) = \sum_{i=1}^{N} \eta_i A\ cos(2\pi f_c(t-\tau_i)) \tag{3}$$

where η_i and τ_i represent the attenuation factor and propagation time for the i^{th} path. Now, when a person walks towards the doorway during such a radio transmission, she will reflect a signal which will arrive at the receiver with a frequency (f_c') larger than the transmitted frequency. This is given by

$$y'(t) = \eta A\ cos(2\pi f_c'(t-\tau)) \tag{4}$$

This frequency difference (Δf) between the transmitted (f_c) and received frequency (f_c') is referred to as the *Doppler shift*. The Doppler shift caused by a target moving at velocity v at an angle θ relative to the receiver, is given by [47]

$$\Delta f = \frac{2 * f_c * v * cos\theta}{c} \tag{5}$$

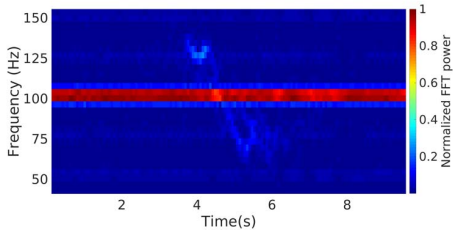

Fig. 3: Each receiver computes an *amplitude spectrogram* - a measure of the strength of each frequency component over time. The faint signal on either side of the baseband tone shows the Doppler reflections due to a human walking through the doorway[1].

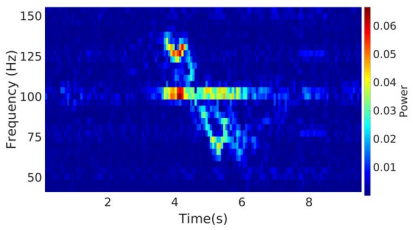

Fig. 4: Each receiver performs spectrogram enhancement on the amplitude spectrogram resulting in a more visible Doppler signal, and baseband tone mitigation.

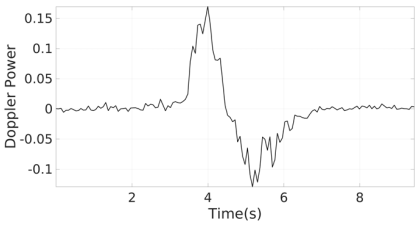

Fig. 5: The Doppler Power (DP) is a measure to infer the moment, the person crosses the sensor. There is positive DP when the person approaches the doorway, and negative DP when the person exits. Hence, the zero-crossing of DP tells us when the person crosses the sensor.

where f_c is the transmitter's center frequency and c is the speed of light in the transmission medium. Given a center frequency of 2.4GHz, and an average human walking speed of 1.2 to 1.3 ms^{-1} [48], the maximum Doppler shift will be about 21Hz. Similarly, when the person walks away from the doorway during an RF transmission, her reflection will arrive at the receiver with a frequency less than the transmitted frequency, resulting in a *negative Doppler shift*.

Doorpler captures the *positive Doppler shift* in order to detect a crossing (*negative Doppler* happens after the person has crossed the doorway threshold). It does so in two steps. First, it tries to extract y'(t) from the received signal via a Butterworth bandpass filter (cutoff frequency of 3 to 25Hz), such that only the reflection from the human remains. Next, it obtains the envelope of the filtered signal, and detects a crossing only when the envelope power is larger than a threshold (set as 5 times the noise-floor). Fig. 1 shows the envelope power of the Doppler filtered signal for 12 doorway crossings. We can clearly see that the envelope power during a crossing is much larger than that during a crossing absence. The advantage of this technique is also that both the filtering and the envelope detection can be performed entirely in analog at just a few microwatts of power [49], [50].

When a potential crossing is detected, the 2.4GHz sensor triggers on a higher power 5.8GHz radio array. The 5GHz radio performs two tasks - (i) direction estimation, and (ii) crossing confirmation. Crossing confirmation is necessary because the crossing detected via the above technique by the 2.4GHz radio can result in false positives. This is because any approaching movement by a person towards the doorway, when she is close to the doorway can cause positive Doppler. For example, all cases shown in Fig. 2 will result in positive Doppler (until the person reaches the line of the receiver), followed by a negative Doppler. However, only cases (i) and (ii) are true doorway crossing events. As the above approach will treat all 6 cases to be true crossing events, the 5GHz radio is used to filter out these false positive cases.

[1] All spectrogram figures are best viewed in color.

B. Direction Estimation

The triggered 5.8GHz receiver-array is used for direction estimation. We point out that *Doorpler* cannot simply use positive and negative Doppler to obtain direction because irrespective of which side the person crosses the doorway from, she will cause positive Doppler during approach and a negative Doppler during exit. As a result, *Doorpler* estimates the direction of the person crossing the doorway by calculating the *angle-of-arrival* (AoA) of the weak reflected signal coming off the human. The AoA of this signal will be positive when the person is on one-side of the doorway, and negative when the person is on the other side. Finally, *Doorpler* fuses angle estimates from multiple (four) antennas in order to improve the direction estimate. Given this overview, we next explain the details of *Doorpler's* direction estimation.

Upon being triggered by the 2.4GHz radio, each element of the 5.8GHz array transforms the received multipath-rich raw time-domain baseband samples into spectrograms via the Short Time Fourier Transform (STFT). The STFT essentially employs a sliding window over the received time-domain samples and then performs a Fast Fourier transform (FFT) on each window. The resulting spectrogram is essentially a three dimensional plot representing the frequency domain of the received signal over time (i.e. x-axis is time, y-axis is frequency and z-axis is corresponding metric that is analyzed, namely amplitude or starting phase of the signal). We henceforth refer to the spectrogram with an amplitude z-axis as the *amplitude spectrogram*, the one with a phase z-axis as the *phase spectrogram*, and so on. For example, Fig. 3 shows an example of an amplitude spectrogram.

Step 1: Compute Amplitude Spectrogram - At first, each array element computes an *amplitude spectrogram* (Fig. 3). Each cell (i,j) represents the power of a certain frequency component at a given time. The strong signal at the center of this spectrogram represents the transmitted signal and its multipath reflections (Equation 3). The thin contour (4 to 6s) around it shows the Doppler reflections (Equation 4) of a human walking through the doorway. In the frequency domain, a spectrogram stretches from 0 to S Hz, where S is the baseband sampling rate. Not all these frequencies are of

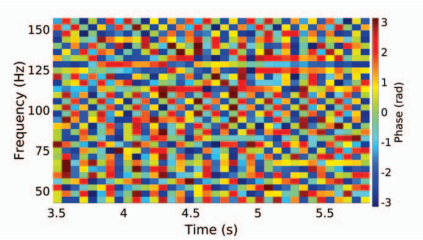

Fig. 6: Each receiver computes a *phase spectrogram* indicative of the starting phase of each frequency component over time. The phase spectrogram by itself is not very useful, but phase difference computed on a pair of antennas reveals useful direction information.

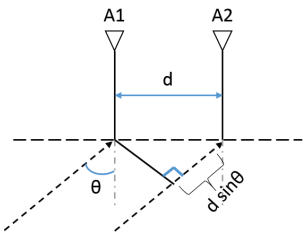

Fig. 7: If two antennas are separated by a distance *d*, then a signal incident at angle θ, travels an extra distance of d sinθ to the second antenna. This results in an instantaneous phase difference of 2π*d*sinθ/λ between the two antennas.

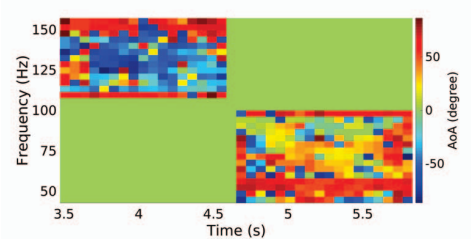

Fig. 8: Each receiver pair computes an angle-of-arrival (AoA) spectrogram on either side of the doorway crossing point. The AoA of the Doppler signal is predominantly negative when the person is on one side of the doorway, and positive when she is on the other side.

interest - i.e. we only care about the frequencies around the transmitted tone frequency where the Doppler shifts occur. From Equation 5, for an average human walking speed of 1.3m/s during a 5.8GHz RF transmission, this corresponds to a Doppler shift of about 50Hz. As a result, *Doorpler* only considers a "smaller" amplitude spectrogram that is +/- 50Hz around the transmitted baseband tone frequency (f_{tone}). We refer to this frequency range as f_{min} *to* f_{max}. This reduces the computational load on the microcontroller that performs the digital baseband processing.

Step 2: Perform Spectrogram Enhancement - The Doppler reflected signals in the frequency bands around the transmitted tone are extremely faint. Consequently, each receiver performs spectrogram enhancement [51], [52] on the aforementioned amplitude spectrogram in order to extract the weak Doppler signal. This is done by first normalizing the amplitude spectrogram with respect to each time bin (i.e. a normalization per column). As a result of this step, the tone-band will have the highest (unit) magnitude. Next, we subtract each column (frequency) of this computed spectrogram from a background column-vector. This background column vector is computed by averaging a similarly normalized background spectrogram of 5 seconds (that is computed initially). Consequently now, the tone band gets mitigated, and the Doppler bands become "visible", during motion. Fig. 4 shows an example of an enhanced amplitude spectrogram ($AS_{enh}(f,t)$), and we see the Doppler bands becoming more visible.

Step 3: Identify Zero Crossing - In order to compare the AoA of the human-reflected signal on each side of the doorway, *Doorpler* first determines the moment the person was at the doorway (i.e. underneath the sensor). It does so by identifying the point of transition from positive to negative Doppler (similar to pseudo-Doppler direction finding radars [26]). It identifies this Doppler transition point by computing a measure called *Doppler Power* (DP). This measure is obtained by weighting the power value from the enhanced amplitude spectrogram with the corresponding Doppler sign (+1 for positive Doppler bands and -1 for negative Doppler bands). More formally,

$$DP(t) = \sum_{f=f_{min}}^{f_{max}} sign(f) \times AS_{enh}(f,t), \tag{6}$$

$$\text{where } sign(f) = \begin{cases} +1, f > f_{tone}\ (Positive\ Doppler) \\ -1, f < f_{tone}\ (Negative\ Doppler) \end{cases}. \tag{7}$$

Intuitively, the above is a measure that captures the cumulative Doppler power (in the frequency bands corresponding to human motion), factoring in the manner of movement (approach v/s exit). Via this measure, a person approaching the doorway causes positive Doppler Power, while a person exiting causes negative Doppler Power. Hence, if we calculate Doppler Power over the entire crossing duration, then the zero-crossing would give us the Doppler transition point. Fig. 5 shows the Doppler Power during a doorway crossing for one of the antennas. In this figure, we can clearly see the zero-crossing of interest around 4.5 second. *Doorpler* determines this zero-crossing point via a technique similar to FormaTrack [7]. We denote this zero-crossing time as T_{cross}.

Step 4: Compute Phase Spectrogram - Having determined the moment the person is in the doorway, *Doorpler* next determines the direction of transition. As mentioned before, *Doorpler* determines direction by computing the AoA of the human-induced reflection. To measure this AoA, each array element first computes a *phase spectrogram* – x-axis is time, y-axis is frequency and z-axis is the starting phase of the signal. Fig. 6 shows an example of a phase spectrogram at a receiver, which appears to reveal little information.

However, as seen in Fig. 7, when two antennas A1 and A2 are placed at a distance *d* apart, a signal arriving at an angle θ to the antennas will travel an extra distance of *d sin*θ to A2. This additional distance results in an instantaneous phase difference [28] between the two antennas of $\Delta\phi = \frac{2*\pi*d*sin*\theta}{\lambda}$, where λ is the carrier wavelength (=5.17cm for a 5.8GHz signal). When d is half-wavelength ($\lambda/2$), the AoA is given by

$$\theta = \arcsin\frac{\Delta\phi}{\pi} \tag{8}$$

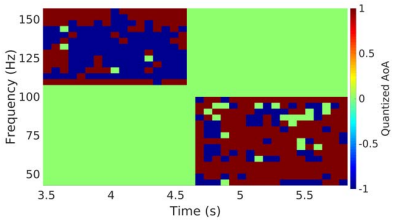

Fig. 9: Since *Doorpler* only cares about the direction of doorway transition, each receiver pair quantizes the AoA estimates to -1, 0 or +1, depending on the sign of the AoA.

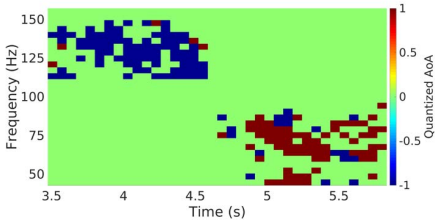

Fig. 10: *Doorpler* mitigates the effect of secondary Doppler reflections by fusing AoA estimates from multiple antenna pairs. It computes a *consensus spectrogram* where each quantized AoA cell must be agreed upon by all antenna pairs.

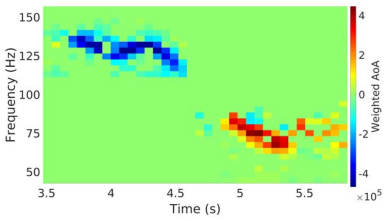

Fig. 11: *Doorpler* further reduces the effect of secondary reflections by weighting the consensed quantization with the corresponding power value from all the receivers. Consequently, Doppler reflections coming straight from the human get weighted higher than the secondary Doppler reflections.

Consequently, *Doorpler* takes the *phase spectrogram* for two successive receivers (i.e.λ/2 apart) , and calculates the phase difference ($\Delta\phi$) between them at every spectrogram cell. This results in a *phase difference spectrogram*, for every antenna pair.

However, the received signal in an antenna is the superposition of multiple paths, and hence the above equation breaks down if applied directly on the received signal. To isolate the reflection from the moving target alone, *Doorpler* computes the phase difference only in the Doppler bands (+/- 6Hz to +/- 50Hz from the tone frequency), leveraging the intuition that the Doppler reflections come from the moving human. We mitigate the effect of secondary reflections - i.e. transmitter –> human –> environment –> receiver via Step 7.

Step 5: Compute Angle-of-Arrival (AoA) Spectrogram - From each computed *phase difference spectrogram*, *Doorpler* next computes an AoA spectrogram based on Equation 8. Intuitively, it is the AoA of the Doppler induced reflection (when it exists), for each time step. Next, we leverage the fact that a person causes positive Doppler while approaching the doorway, and negative Doppler while exiting. Consequently, the AoA spectrogram is only computed in the positive Doppler bands before the person reaches the doorway (i.e. T_{cross}), and in the negative Doppler bands after the person exits the doorway. More formally, given a phase difference spectrogram $\Delta\phi_{sgram}$, the AoA spectrogram AoA_{sgram} is given by

$$AoA_{sgram}(f,t) = \begin{cases} \arcsin\frac{\Delta\phi(f,t)}{\pi}, & if\ (i)\ f > f_{tone}\ and\ t < T_{cross} \\ & (ii)\ f < f_{tone}\ and\ t > T_{cross} \\ 0 & , else \end{cases} \tag{9}$$

Fig. 8 shows an example of an AoA spectrogram. We can see that the AoA in the Doppler bands are mostly on one-side of 0°before T_{cross} (around 4.5 seconds), and on the other side of 0°after T_{cross}.

Step 6: Obtain Quantized AoA Spectrogram - In order to determine the direction of doorway transition, *Doorpler* only needs to know if the human reflection is at a positive or negative angle. Consequently, *Doorpler* quantizes the computed AoA spectrogram such that the cells with positive and negative angles are set to +1 and -1 respectively. This results in the *Quantized AoA spectrogram*, as shown in Fig. 9.

Step 7: Secondary Reflections Mitigation - In order to mitigate the effect of secondary reflections coming from the human, *Doorpler* fuses data from multiple antenna pairs. It leverages the intuition that as a person walks through the doorway, there will be a few "good" reflection points where the person reflects directly to the radar [12]. With the antennas located in far-field, all pairs will agree on the angle quantization at these reflection points. Consequently, *Doorpler* forms a *consensus spectrogram* wherein each cell (i,j) has a quantized angle only when agreed upon by all receiver pairs. The *consensus spectrogram* in Fig. 10 shows a reduction in the number of bad angle estimates, compared to Fig. 9.

The *consensus spectrogram* could have certain 'bad' cells which do not agree with the actual direction of doorway crossing because of noise. However, these noisy cells have low power if they are not a reflection from the human. Consequently, we eliminate these noisy cells by weighting each cell (i,j) of the *consensus spectrogram* with the corresponding power value obtained by summing the (i,j)th cell in the *amplitude spectrogram* of all the antenna pairs. This step further mitigates secondary reflections as they will have lower power compared to those coming directly off the person. Fig. 11 shows the spectrogram after amplitude-weighting which exhibits a clear difference on the two sides of the doorway. (amplitude-weighting increases the recall by about 20%). Formally, if *CS* represents the *consensus spectrogram*, and AS_n represents the amplitude spectrogram of the nth receiver, then the resulting *amplitude weighted consensus spectrogram* (CS_{wt}) is given by

$$CS_{wt}(f,t) = CS(f,t) * (\sum_{n=1}^{N} AS(f,t)) \tag{10}$$

, where N is the number of receivers.

Step 8: Sign comparison - Finally, *Doorpler* determines the direction of transition by comparing the sum of the submatrices, pre and post doorway crossing (i.e. the left and right half of CS_{wt}). This weighted sum will change from positive to negative when the person walks from one side of the doorway to another, and from negative to positive, when she walks the other way. More formally, if we define transition from the

(a) *Doorpler* was mounted atop an office doorway. A scripted study and an 80-hour in-situ study was performed on this doorway yielding over 1500 doorway crossing events.

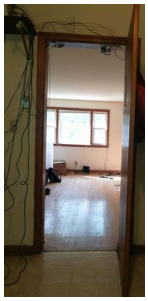

(b) *Doorpler* was mounted atop the most commonly used doorway in a 2-person home for 120 hours yielding 113 doorway crossing events.

Fig. 12: Experimental Setup

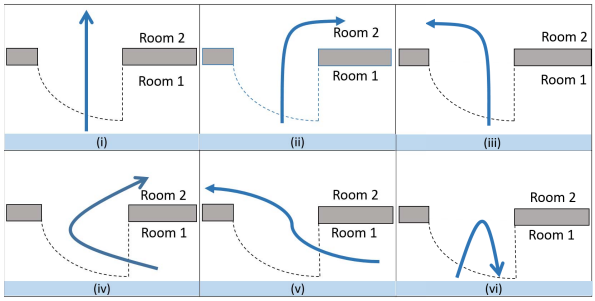

Fig. 13: In the scripted study, participants walked through the instrumented doorway in 6 different ways yielding 1440 crossings.

positive to the negative side as IN, and vice versa as being OUT, then the direction estimate is given by

$$Dir = \begin{cases} IN & , if \sum_{t<t_{cross}} CS_{wt}(f,t) > 0 \; and \sum_{t>t_{cross}} CS_{wt}(f,t) < 0 \\ OUT, & if \sum_{t<t_{cross}} CS_{wt}(f,t) < 0 \; and \sum_{t>t_{cross}} CS_{wt}(f,t) > 0 \end{cases}$$

Step 9: Crossing Confirmation - As mentioned earlier, the 2.4GHz radio which performs crossing detection based on positive Doppler shifts can trigger false positives for near-door events such as hovers and U-turns. These false positives are eliminated via the sign comparison in Step 9. If the weighed sums on either side of the doorway crossing point are both positive (or) both negative, then *Doorpler* perceives that the person did not actually cross the doorway, and discards the event.

Finally, we also point out that we have a layered approach (i.e. 2.4GHz triggering on the 5GHz array) because a 2.4GHz phased array with four antenna elements placed half-wavelength apart will occupy a total of 18.75cm. This is longer than most doorjamb widths [23]. A 5.8GHz array on the other hand occupies a much smaller width spanning just 7.8cm, which can fit atop most doorways.

IV. Experimental Setup

To test our hypothesis, we implement the 2.4 GHz and the 5.8 GHz RF transceivers using software defined radios. The

Participant	P1	P2	P3	P4	P5	P6	P7	P8
Height (cm)	161	167	168	170	172	175	177	181
Weight (kg)	60.8	61.0	56.1	78.0	56.7	97.9	82.5	80.0

TABLE I: The height and weight of the 8 participants who walked through an instrumented office doorway for 6 days generating 1440 doorway crossing events

2.4 GHz transmitter and receiver were realized by two USRP N210s [53] with an SBX daughterboard [54] each. The 5.8 GHz transmitter was implemented on a USRP N210 with a CBX daughterboard [55]. The 4-element 5.8 GHz receiver array was implemented on a USRP X310 [56] with two TwinRX daughterboards [57] that provide four phase-coherent RF receive chains. Each transceiver pair was frequency synchronized via a common reference clock, Octoclock-G [58]. Without frequency synchronization, the *Doppler* signal gets submerged in the carrier frequency difference between the transceivers (*Carrier Frequency Offset* [59]). The receivers were time synchronized (sample-aligned) via a pulse-per-second signal provided by the same Octoclock-G. The 5.8GHz transmitter loaded a 100 Hz baseband tone on its carrier whose Doppler was analyzed for both crossing confirmation and direction estimation. Both transmitters transmitted at just -10dBm (100μW) transmit power, while the receivers sampled at 250Hz. Each RF chain was terminated by a 3dBi omni-directional antenna, and these antennas were mounted atop a doorway as shown in Fig. 12a and Fig. 12b. The transmit and receive antennas were mounted in a *gain-mismatch* fashion (pointing at each other so that the nulls align). This reduced the direct path by 10.2dB. The antennas in the 5.8 GHz phased-array are placed half-wavelength apart (2.58cm).

Finally, there is a constant but repeatable phase-offset between each of the 5.8 GHz receive-chains due to the different local oscillators involved. These phase offsets were eliminated via a one-time calibration [28]. The phase offset if left uncalibrated, would appear as an added phase difference in Equation 8, resulting in an incorrect angle estimate. We performed two sets of studies with this setup :

1. A scripted study was performed on an office doorway (Fig. 12a), involving 8 participants of varying heights and weights as shown in Table I. The participants were asked to walk for 6 days through the instrumented doorway. On each day, each participant walked 6 times (3 times back and forth) through the doorway in the 6 ways shown in Fig. 13. No restrictions were imposed on the type of clothing the participants wore, or the time of the experiment. In all, this study yielded 1440 doorway crossings (+ 144 U-turn events).

2. Two sets of in-situ experiments were performed. A first in-situ study was performed on the same office door for 80 hours which yielded 133 doorway crossings. A second in-situ study was performed on the most commonly used doorway in a 2-person home (Fig. 12b). This study was performed for 120 hours, and resulted in 113 doorway crossing events.

The crossings were recorded by a video camera pointed at the doorway, which were then manually analyzed. We evaluate *Doorpler* accuracy via four metrics:

- *Recall*: The fraction of actual doorway crossings that

Study \ Metric(%)	Recall	Precision	DirAcc	EffDirAcc
Scripted	99.0	99.9	100.0	99.6
In-situ	95.4	98.7	100.0	98.0

TABLE II: *Doorpler* achieves over 99% accuracy across all metrics of interest in the scripted study. It also achieves an average accuracy of over 95% across all metrics in the 200 hours of in-situ data.

were correctly detected by *Doorpler*.

- *Precision*: Amongst the doorway crossings detected by *Doorpler*, the fraction that actually occurred.
- *Direction Accuracy* (DirAcc): The fraction of correctly detected doorway crossings having the correct direction.
- *Effective Direction Accuracy* (EffDirAcc): The crossing confirmation (Section III-B) depends on the direction estimate. Consequently, an incorrect direction estimate can manifest itself as a false negative, false positive or a direction error. This metric captures this manifestation as the mean of *recall*, *precision* and *direction accuracy*.

V. Evaluation

A. Doorpler Accuracy

Table II shows that *Doorpler* achieved over 99% and 95% accuracy across all metrics of interest in the scripted and in-situ study respectively. The missed detections in the in-situ study are attributable to the following causes: (a) two people walking one behind the other through the doorway (occlusion), (b) several cases of people walking all the way up to the door, talking to someone in the room for a few seconds, and then continuing motion into the room, (c) direction-errors (i.e. a true crossing event was incorrectly detected as a U-turn/near-door event), (d) not all the 5GHz radio chains were triggered because of the conservative threshold that trades-off precision and recall, and finally (e) a case of a person located very close to the doorway, walks through the doorway. In this case, the positive Doppler received by the 2.4GHz radio was not significant. The causes for the 3 false detections over the 200 hours of data collection were due to direction errors (i.e. a U-turn/near-door event was not detected). In all these cases, the weighted consensus sum on one of the sides was only marginally greater (or lesser) than zero. We leave it as a future work to filter out these low-confidence crossing events.

B. Power Consumption

We next study the power consumption of *Doorpler*. We cannot take power numbers directly from the USRPs as they are over-engineered for our use-case. For e.g., the components in its radio chain (i) operate over a multi-GHz band (while we operate at a single frequency), (ii) can transmit at over +10dBm (we transmit 100x lower at -10dBm), (iii) can receive signals as low as -130dBm (a human reflection 1m away from the setup comes at -66dBm [60]), (iv) has an ADC with a sampling rate of 200MHz (we sample at 250Hz), etc. Consequently, we come up with an equivalent realization of *Doorpler* based on the USRP radio chain, and obtain power numbers of this realization from literature. We leave it as a future work to engineer the analog integrated system based on the provided design. Fig. 14 shows a high-level block diagram of *Doorpler*'s power hungry RF components with the 2.4GHz RF chain waking up the 5GHz array upon crossing detection.

2.4GHz radio : Liu et al. [61] built a -10dBm RF front-end similar to *Doorpler* for Bluetooth Low Energy, Zigbee and Medical Body Area Network applications. It consumes 4.6mW for transmission and 3.8mW for reception. However with shareable components like the oscillator, the power consumption becomes 6.6mW. In our studies, we observed that the 2.4GHz radios can be 15% duty-cycled without accuracy loss. This results in a power-consumption of 5.8mW. We point out that this system exceeds *Doorpler's* necessity. For e.g., the receiver sensitivity is -96dBm (*Doorpler* is about -61dBm), the data rate is over 950Kbps (*Doorpler* samples at just 250 samples/sec, i.e. 2Kbps), the radio chains support modulation techniques like GFSK, DQPSK, etc (*Doorpler* runs on an unmodulated tone). The envelope detector to trigger the 5GHz chain can be realized in tens of microwatts of power [49]. Furthermore, we point out that unlike typical transceivers, we do not require components like the oscillators to be stable over a long-term (as they are shared between TX and RXs). Said differently, *Doorpler* is not drift sensitive, and only cares about short-term stability (crossing duration).

5GHz RF chain : Similarly, Homayoun et al. [62] built a 11.6mW receiver for 802.11a applications. With 4 receive chains, the total power consumption becomes 46.4mW. This receiver has a sensitivity of -70dBm at 54Mbps, and a noise figure of 6dB which exceed *Doorpler's* requirements. The transmitter can be realized via a -7dBm, 13.5mW frequency synthesizer [63], eliminating the need for an on-chip power amplifier, as the output power is high enough. This results in a total power consumption of 59.9mW for the 5GHz chain.

Digital Baseband Processing : To measure the power consumption of the micro-controller unit (MCU), we implemented the digital baseband processing of *Doorpler* on an ultra-low power MCU, MSP432 [64], and measured its power consumption. We observed that the MSP432 consumed 6.4mW of power. This results in a total power consumption of the 5GHz chain of 66.3mW (= 59.9 + 6.4)mW.

Average power and comparison with other doorway tracking systems : The average power consumption of *Doorpler* is given by *(Power Draw of 2.4GHz radio) + (On Time of 5GHz array)*(Power Draw of 5GHz array)*. In our study, we observed that the 2.4GHz radio triggers the array 0.4% of the time. This results in an average power consumption of 6.1 (=5.8 + (0.4% * 66.3)) mW.

Table III compares the power consumption of the triggered component of *Doorpler* with other doorway-tracking systems. We report the power numbers this way as all of these systems can technically be triggered by the 2.4GHz radar, even though it is not part of their setup. From this table, we observe that the triggered component of *Doorpler* consumes 2.3x lower power than the nearest baseline. An alternate way to interpret its advantage is that should *Doorpler* be part of an environment where near-door events occur frequently (e.g., adjacent to a busy hallway), it will result in 2.3x less power consumption

System	Doorjamb [5]	SonicDoor [9]	FORK [6]	PeopleFlow [11]	FormaTrack [7]	Doorjamb 2.0 [8]	Lethe [10]	**Doorpler (5GHz)**
Technology	Ultrasound	Ultrasound	Depth Camera	IR	UWB Radar	Ultrasound + IR	Thermal Camera	**CW Radar**
Power (mW)	150	300	26500*	714.9*	2450*	595.5	300	**66.3***

TABLE III: The triggered component of *Doorpler* (5.8GHz array) consumes 2.3x lesser power than the nearest doorway tracking system (*includes signal processing power consumption when real time claim reported by authors).

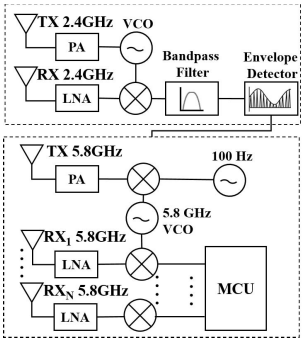

Fig. 14: High-level *Doorpler* block diagram: The lower power 2.4GHz radio triggers the higher power 5.8GHz chain upon crossing detection.

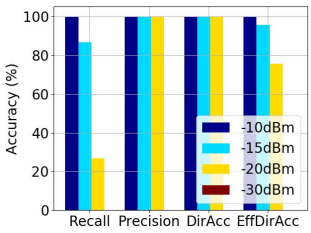

Fig. 15: As the transmit power of *Doorpler* is reduced, the accuracy starts to decrease. This is because the reflected Doppler signal becomes weaker and starts to submerge itself in the noise-floor.

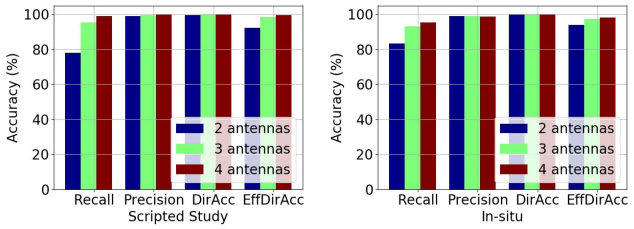

Fig. 16: Effect of number of receive chains : The recall and effective direction accuracy increase as we add more receivers. This is because AoA errors made by a single receive pair get mitigated while taking a consensus. *Doorpler* uses 4 receive chains.

each time it is triggered by a person walking close to the door in the hallway. Furthermore as mentioned in Section II, *Doorpler* being an RF-based system does not suffer from many of the limitations of other doorway tracking systems.

Energy harvesting feasibility: Prior work [20] has shown that indoor incident solar irradiation varies from 11-115μW/cm^2. Given a 1m x 10cm solar panel of with 20% efficiency, mounted in the doorway, this translates to a power supply of 2.2 to 23mW. Consequently, *Doorpler's* demand of 6.1mW can be satisfied by many of the doorways. For those doorways with low irradiance, *Doorpler* could still potentially be harvestable by placing larger solar panels and/or placing them above the door frame on either side of the doorway. From Table III, we also point out that *Doorpler* can be within the harvestable range so long as the 5GHz radio chain is triggered for less than 32% (=23mW/(5.8+66.3)mW) of the time.

C. *Real-timeness of* Doorpler

We next evaluate if *Doorpler* can operate in real-time by measuring the run-time of the baseband processing on the MSP432. We observed that the direction can be estimated by the MSP432 at an average of *13.8*ms. With 750ms of crossing data (Section V-F) on each side of the doorway needed to achieve a high accuracy, a direction estimate can be provided just 763.8ms(=750+13.8ms) after the person crosses the sensor. Anecdotally, at an average walking speed of 1.2m/s, a human covers just over a step within a 763ms duration. Thus, *Doorpler* can enable several real-time smart home applications like smart-lighting or automatic HVAC control. From an implementation perspective, to save memory on the MCU, steps 1, 2, 4 to 6 of Section III-B were implemented in a streaming manner (i.e. per arriving FFT frame).

D. *Effect of Number of Receive Chains*

The number of receivers has an impact on the total power consumption of *Doorpler*. From Fig. 16, we see that the recall and effective direction accuracy increases as we add more receivers. This is because AoA errors made by a single receiver pair gets mitigated during consensus. We point out that there is an inherent *power-accuracy trade-off* here - with more receivers, even though the accuracy increases, the power consumption also increases by 11.6mW for every RX-chain. However, *Doorpler* still uses all 4 RX-chains because the array comes on for only a small fraction (0.4%) of the time.

E. *Effect of Transmit Power*

We next study the effect of lowering the transmit power, as a lower transmit power typically results in lower power consumption [44]. One person was asked to walk a total of 120 times in varying directions (Fig. 13), through an instrumented doorway (Fig. 12b). Fig. 15 shows that as we lower the transmit power from -10dBm to -30dBm (by attaching attenuators), the ability to detect crossings decreases. This is because the reflected Doppler becomes weaker and submerges itself in the noise-floor. The precision and direction accuracy do not suffer because the fraction of crossings detected is low. As before, there is a power-accuracy tradeoff here. However, the accuracy gain by transmitting at -10dBm outweighs the power benefits at -15dBm and lower. Hence, *Doorpler* transmits at -10dBm.

F. *Effect of Wake-up Time*

We next study the effect of the wake-up time of the 5GHz chain on accuracy and timing. If the 2.4GHz radio triggers too late, then the Doppler is not significant (θ ˜= 0°), while if it triggers too early then noisy spectrogram cells, or data from a prior crossing starts to dominate. From Fig. 17, we observe that the 5GHz array can be woken up as late as 750ms before a doorway crossing event. This also says that any future work that replaces the 2.4GHz radio with an alternate sensor must ensure that the 5GHz array is woken up at least 750ms before

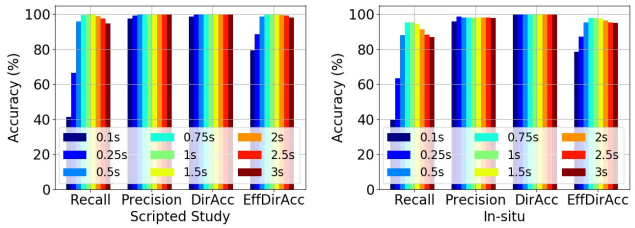

Fig. 17: The 5GHz array works with high accuracy as long as it is triggered at least 750ms before the person crosses the doorway. With a late trigger, the accuracy suffers because the Doppler is not significant. With an early trigger, the accuracy suffers as noisy spectrogram cells, or data from a prior crossing starts to dominate.

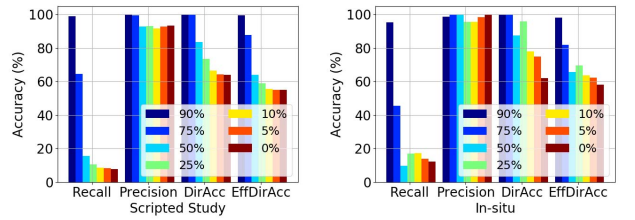

Fig. 18: As the degree of overlap between FFT samples in the spectrogram decreases, the accuracy of *Doorpler* starts to decrease. This is because with lesser overlap, the useful Doppler data gets out-weighed by noisy spectrogram cells.

the person reaches the doorway threshold. Since we consider an equal time window on either side of the doorway crossing point to determine direction, this result places a lower bound on the real-timeness of the system (i.e. at least 750ms after the person crosses the doorway threshold).

G. Effect of Degree of Spectrogram Overlap

The degree of spectrogram overlap is a measure of how often an FFT must be performed by the MCU. A high overlap results in a tighter real-time bound as lesser 'fresh' samples are required for each subsequent FFT (stream processing of Steps 1, 2, 4 to 6). From Fig. 18, we see that as the overlap decreases, the accuracy also starts to decrease. This is because with lower overlap, the useful signal data gets "out-weighed" by the noisy spectrogram cells. Consequently, *Doorpler* uses 90% overlap. Despite the high overlap, the MCU performs all the streaming FFT-related operations on a single batch of 64 samples from all receive chains, on average 13ms before the next set of 6 samples (90% overlap) arrives. A high overlap also results in a higher power draw as the on-time of the MCU increases. This does not impact *Doorpler* as the MCU consumes only 6mW, and the accuracy benefits of a high overlap outweigh the MCU "sleeping" benefits of low overlap.

VI. Discussion

A. Health Concerns of Doorpler

There are no health concerns with *Doorpler* as its Effective Isotropic Radiated Power (EIRP) after accounting for antenna gain and cable loss is just 125μW (-9dBm). In comparison, the maximum FCC permitted transmit power for an indoor 5GHz WiFi access point is 1W [65] (nearly 8000x higher).

B. Building the Integrated System

We have demonstrated that *Doorpler* can perform doorway crossing detection and direction estimation using just a -10dBm tone via software defined radios. However, this prototype is both expensive and bulky. Our next step is to engineer an integrated system based on Section V-B. We would then aim to incorporate it with identity sensing from Doorjamb [5] or FormaTrack [7]. Such a system would take us closer to the vision of *plug-and-play* doorway tracking systems [5], [34].

C. Multi-Person Crossings

Doorpler has trouble when multiple walk through the doorway one behind the other (occlusion), a strong point of FORK [6]. However, this is typically not a common scenario in homes (for instance, in a prior study, the median time gap between two different individuals walking through the same doorway in an 8-room home was 10 minutes [66]).

D. Effect of Pets and Doors

Doorpler can be triggered by crossing pets as they too create Doppler. However, their gait is different from humans [67]. We leave it as a future work to differentiate pets based on gait.

While we do not explicitly consider door interactions in this work, we hypothesize that *Doorpler* can be made to handle the common case of *a person walking up to the door, opening/closing it and continuing* motion. The more challenging scenario occurs when the door moves simultaneously in the direction opposite to human motion, resulting in simultaneous Doppler from both sides. However, this can potentially be addressed by leveraging the cyclicity of human gait. We leave it as a future work to test *Doorpler* with door movements.

VII. Conclusion

In this paper, we present *Doorpler*, a low-power and real-time Doppler-based zone occupancy sensing solution that performs crossing detection and direction estimation using just an RF tone signal. *Doorpler* infers the direction of human transition by computing the angle-of-arrival of the reflection coming from the human. We evaluate *Doorpler* via a scripted study and two in-situ studies. Our results indicate that *Doorpler* can achieve over 99% and 95% accuracy across all metrics of interest in the scripted and in-situ studies, respectively. Our analyses also estimate that an analog realization of *Doorpler* would consume 6.1mW of power, falling in the indoor harvestable solar range. Our implementation of the baseband processing on an ultra low power MCU took 13.8ms, thus having the potential to enable several real-time smarthome applications like smart-lighting, HVAC control, etc.

References

[1] V. Smith, T. Sookoor, and K. Whitehouse, "Modeling building thermal response to hvac zoning," *ACM SIGBED Review*, vol. 9, no. 3, pp. 39–45, 2012.

[2] E. Soltanaghaei and K. Whitehouse, "Walksense: Classifying home occupancy states using walkway sensing," in *Proceedings of the 3rd ACM International Conference on Systems for Energy-Efficient Built Environments*. ACM, 2016, pp. 167–176.

[3] "The rise of living alone," https://bit.ly/2Nvgkpi, Aug. 2018.

[4] "Number of single-person households in the u.s. in 2014, by sex and age," https://www.statista.com/statistics/242025/number-of-single-person-households-in-the-us-by-sex-and-age/, Aug. 2018.

[5] T. W. Hnat, E. Griffiths, R. Dawson, and K. Whitehouse, "Doorjamb: unobtrusive room-level tracking of people in homes using doorway sensors," in *Proceedings of the 10th ACM Conference on Embedded Network Sensor Systems*. ACM, 2012, pp. 309–322.

[6] S. Munir, R. S. Arora, C. Hesling, J. Li, J. Francis, C. Shelton, C. Martin, A. Rowe, and M. Berges, "Real-time fine grained occupancy estimation using depth sensors on arm embedded platforms," in *Real-Time and Embedded Technology and Applications Symposium (RTAS), 2017 IEEE*. IEEE, 2017, pp. 295–306.

[7] A. Kalyanaraman, D. Hong, E. Soltanaghaei, and K. Whitehouse, "Forma track: tracking people based on body shape," *Proceedings of the ACM on Interactive, Mobile, Wearable and Ubiquitous Technologies*, vol. 1, no. 3, p. 61, 2017.

[8] E. Griffiths, A. Kalyanaraman, J. Ranjan, and K. Whitehouse, "An empirical design space analysis of doorway tracking systems for real world environments," *ACM Transactions on Sensor Networks (TOSN)*, vol. 13, no. 4, 2017.

[9] N. Khalil, D. Benhaddou, O. Gnawali, and J. Subhlok, "Nonintrusive occupant identification by sensing body shape and movement," in *Proceedings of the 3rd ACM International Conference on Systems for Energy-Efficient Built Environments*. ACM, 2016, pp. 1–10.

[10] E. Griffiths, S. Assana, and K. Whitehouse, "Privacy-preserving image processing with binocular thermal cameras," *Proceedings of the ACM on Interactive, Mobile, Wearable and Ubiquitous Technologies*, vol. 1, no. 4, p. 133, 2018.

[11] H. Mohammadmoradi, S. Munir, O. Gnawali, and C. Shelton, "Measuring people-flow through doorways using easy-to-install ir array sensors," in *Distributed Computing in Sensor Systems (DCOSS), 2017 International Conference on*, 2017.

[12] F. Adib, C.-Y. Hsu, H. Mao, D. Katabi, and F. Durand, "Capturing the human figure through a wall," *ACM Transactions on Graphics (TOG)*, vol. 34, no. 6, p. 219, 2015.

[13] A. Dersan and Y. Tanik, "Passive radar localization by time difference of arrival," in *Military Communications Conference (MILCOM 2002)*. IEEE, 2002, pp. 1251–1257.

[14] S. Brown, J. Irvine, and A. Metcalfe, "Antenna characterisation for amplitude comparison in electronic warfare systems," 2010.

[15] R. J. Mailloux, *Phased array antenna handbook*. Artech House Boston, 2005, vol. 2.

[16] R. Schmidt, "Multiple emitter location and signal parameter estimation," *IEEE transactions on antennas and propagation*, vol. 34, no. 3, pp. 276–280, 1986.

[17] R. Roy and T. Kailath, "Esprit-estimation of signal parameters via rotational invariance techniques," *IEEE Transactions on acoustics, speech, and signal processing*, vol. 37, no. 7, pp. 984–995, 1989.

[18] J. Ansari, D. Pankin, and P. Mähönen, "Radio-triggered wake-ups with addressing capabilities for extremely low power sensor network applications," *International Journal of Wireless Information Networks*, vol. 16, no. 3, p. 118, 2009.

[19] M. Del Prete, D. Masotti, A. Costanzo, M. Magno, and L. Benini, "A dual-band wake-up radio for ultra-low power wireless sensor networks," in *Wireless Sensors and Sensor Networks (WiSNet), 2016 IEEE Topical Conference on*. IEEE, 2016, pp. 81–84.

[20] L. Yerva, B. Campbell, A. Bansal, T. Schmid, and P. Dutta, "Grafting energy-harvesting leaves onto the sensornet tree," in *Proceedings of the 11th international conference on Information Processing in Sensor Networks*. ACM, 2012, pp. 197–208.

[21] S. Blackman and R. Popoli, "Design and analysis of modern tracking systems (artech house radar library)," *Artech house*, 1999.

[22] P. J. Gething, *Radio direction finding and superresolution*. IET, 1991, no. 33.

[23] "Typical doorjamb sizes," http://www.doornmore.com/help/jamb-width.html, Aug. 2018.

[24] D. Short, "Radar scan strategies for the patrick air force base weather surveillance radar, model-74c, replacement," 2008.

[25] H. Griffiths and C. Baker, "The signal and interference environment in passive bistatic radar," in *Information, Decision and Control, 2007. IDC'07*. IEEE, 2007, pp. 1–10.

[26] W. Read, "Review of conventional tactical radio direction finding systems," Tech. Rep., 1989.

[27] "Panasonic pir motion sensor brochure," https://www.mouser.com/pdfdocs/PanasonicPIRSensorsBrochure.pdf/, Aug. 2018.

[28] J. Xiong and K. Jamieson, "Arraytrack: A fine-grained indoor location system." in *NSDI*, 2013, pp. 71–84.

[29] D. Vasisht, S. Kumar, and D. Katabi, "Decimeter-level localization with a single wifi access point," in *13th USENIX Symposium on Networked Systems Design and Implementation (NSDI 16)*. USENIX Association, 2016, pp. 165–178.

[30] M. Kotaru, K. Joshi, D. Bharadia, and S. Katti, "Spotfi: Decimeter level localization using wifi," in *ACM SIGCOMM Computer Communication Review*, vol. 45, no. 4. ACM, 2015, pp. 269–282.

[31] S. Kumar, S. Gil, D. Katabi, and D. Rus, "Accurate indoor localization with zero start-up cost," in *Proceedings of the 20th annual international conference on Mobile computing and networking*. ACM, 2014, pp. 483–494.

[32] J. Xiao, Z. Zhou, Y. Yi, and L. M. Ni, "A survey on wireless indoor localization from the device perspective," *ACM Computing Surveys (CSUR)*, vol. 49, no. 2, p. 25, 2016.

[33] E. Soltanaghaei, A. Kalyanaraman, and K. Whitehouse, "Multipath triangulation: Decimeter-level wifi localization and orientation with a single unaided receiver," in *Proceedings of the 16th Annual International Conference on Mobile Systems, Applications, and Services*. ACM, 2018, pp. 376–388.

[34] T. W. Hnat, V. Srinivasan, J. Lu, T. I. Sookoor, R. Dawson, J. Stankovic, and K. Whitehouse, "The hitchhiker's guide to successful residential sensing deployments," in *Proceedings of the 9th ACM Conference on Embedded Networked Sensor Systems*. ACM, 2011, pp. 232–245.

[35] F. Adib, Z. Kabelac, and D. Katabi, "Multi-person localization via rf body reflections." in *NSDI*, 2015, pp. 279–292.

[36] F. Adib, Z. Kabelac, D. Katabi, and R. C. Miller, "3d tracking via body radio reflections." in *NSDI*, vol. 14, 2014, pp. 317–329.

[37] F. Adib and D. Katabi, *See through walls with WiFi!* ACM, 2013, vol. 43, no. 4.

[38] X. Li, S. Li, D. Zhang, J. Xiong, Y. Wang, and H. Mei, "Dynamic-music: accurate device-free indoor localization," in *Proceedings of the 2016 ACM International Joint Conference on Pervasive and Ubiquitous Computing*. ACM, 2016, pp. 196–207.

[39] J.-P. Vasseur and A. Dunkels, *Interconnecting smart objects with ip: The next internet*. Morgan Kaufmann, 2010.

[40] U. A. Perez, "Low power wi-fi: A study on power consumption for internet of things," *Master's Thesis, Facultat dInformàtica de Barcelona (FIB), Universitat Politècnica de Catalunya (UPC), BarcelonaTech*, 2015.

[41] L. L. L. Kan, D. M. Lau, S. Lou, A. W. Ng, R. D. Wang, G. W.-K. Wong, P. Y. Wu, H. Zheng, V. S.-L. Cheung, and H. C. Luong, "A 1-v 86-mw-rx 53-mw-tx single-chip cmos transceiver for wlan ieee 802.11 a," *IEEE journal of solid-state circuits*, vol. 42, no. 9, pp. 1986–1998, 2007.

[42] R. Nandakumar, V. Iyer, D. Tan, and S. Gollakota, "Fingerio: Using active sonar for fine-grained finger tracking," in *Proceedings of the 2016 CHI Conference on Human Factors in Computing Systems*. ACM, 2016, pp. 1515–1525.

[43] R. Nandakumar, A. Takakuwa, T. Kohno, and S. Gollakota, "Covertband: Activity information leakage using music," *Proceedings of the ACM on Interactive, Mobile, Wearable and Ubiquitous Technologies*, vol. 1, no. 3, p. 87, 2017.

[44] R. Rajan and C. Microsemi, "Ultra-low power short range radio transceivers," *Microsemi CMPG, May*, 2012.

[45] R. W. Heath, *Introduction to Wireless Digital Communication: A Signal Processing Perspective*. Prentice Hall, 2017.

[46] T. Wei and X. Zhang, "mtrack: High-precision passive tracking using millimeter wave radios," in *Proceedings of the 21st Annual International Conference on Mobile Computing and Networking*. ACM, 2015, pp. 117–129.

[47] W. G. Carrara, R. S. Goodman, and R. M. Majewski, *Spotlight synthetic aperture radar*, 2007.

[48] T. Oberg, A. Karsznia, and K. Oberg, "Basic gait parameters: reference data for normal subjects, 10-79 years of age." *Journal of rehabilitation research and development*, vol. 30, no. 2, p. 210, 1993.

[49] B. Kellogg, V. Talla, and S. Gollakota, "Bringing gesture recognition to all devices." in *NSDI*, vol. 14, 2014, pp. 303–316.

[50] A. Hylamia, A. Varshney, A. Soleiman, P. Papadimitratos, C. Rohner, and T. Voigt, "Towards battery-free radio tomographic imaging," in

Proceedings of the 11th ACM Conference on Security & Privacy in Wireless and Mobile Networks. ACM, 2018, pp. 293–295.

[51] W. Wang, A. X. Liu, and M. Shahzad, "Gait recognition using wifi signals," in *Proceedings of the 2016 ACM International Joint Conference on Pervasive and Ubiquitous Computing*. ACM, 2016, pp. 363–373.

[52] Y. Ephraim and D. Malah, "Speech enhancement using a minimum-mean square error short-time spectral amplitude estimator," *IEEE Transactions on acoustics, speech, and signal processing*, vol. 32, no. 6, pp. 1109–1121, 1984.

[53] "Usrp n210," https://www.ettus.com/product/details/UN210-KIT, Oct. 2018.

[54] "Sbx daughterboard," https://www.ettus.com/product/details/SBX , Oct. 2018.

[55] "Cbx daughterboard," https://www.ettus.com/product/details/CBX, Oct. 2018.

[56] "Usrp x310," https://www.ettus.com/product/details/X310-KIT, Oct. 2018.

[57] "Twinrx daughterboard," https://www.ettus.com/product/details/TwinRX, Oct. 2018.

[58] "Octoclock-g," https://www.ettus.com/product/details/OctoClock-G, Oct. 2018.

[59] H. Meyr, M. Moeneclaey, and S. Fechtel, *Digital communication receivers: synchronization, channel estimation, and signal processing*. John Wiley & Sons, Inc., 1997.

[60] G. Melia, "Electromagnetic absorption by the human body from 1-15 ghz," Ph.D. dissertation, University of York, 2013.

[61] Y.-H. Liu, X. Huang, M. Vidojkovic, A. Ba, P. Harpe, G. Dolmans, and H. de Groot, "A 1.9 nj/b 2.4 ghz multistandard (bluetooth low energy/zigbee/ieee802. 15.6) transceiver for personal/body-area networks," in *Solid-State Circuits Conference Digest of Technical Papers (ISSCC), 2013 IEEE International*. IEEE, 2013, pp. 446–447.

[62] A. Homayoun and B. Razavi, "A low-power cmos receiver for 5 ghz wlan," *IEEE Journal of Solid-State Circuits*, vol. 50, no. 3, pp. 630–643, 2015.

[63] S. Pellerano, S. Levantino, C. Samori, and A. Lacaita, "A 13.5-mw 5-ghz frequency synthesizer with dynamic-logic frequency divider," *IEEE Journal of Solid-State Circuits*, vol. 39, no. 2, pp. 378–383, 2004.

[64] "Msp432p401r launchpad development kit," http://www.ti.com/tool/MSP-EXP432P401R , Oct. 2018.

[65] "Electronic code of federal regulations," https://bit.ly/2MBPgF8 , Oct. 2018.

[66] A. Kalyanaraman, E. Griffiths, and K. Whitehouse, "Transtrack: Tracking multiple targets by sensing their zone transitions," in *Distributed Computing in Sensor Systems (DCOSS), 2016 International Conference on*. IEEE, 2016, pp. 59–66.

[67] M. Otero, "Application of a continuous wave radar for human gait recognition," in *Signal Processing, Sensor Fusion, and Target Recognition XIV*, vol. 5809. International Society for Optics and Photonics, 2005, pp. 538–549.